

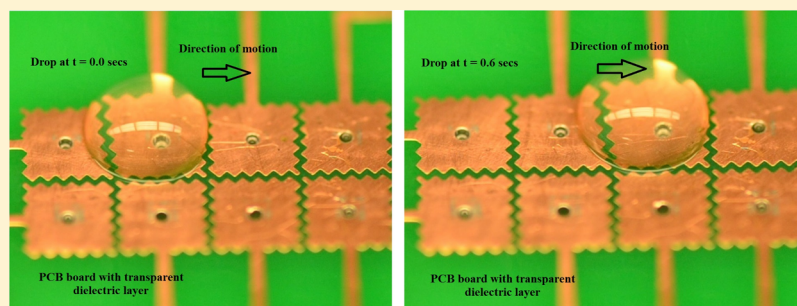
## Control of Direct Written Ink Droplets Using Electrowetting

J. Plog,<sup>†,§</sup> J.-M. Löwe,<sup>†,‡,§</sup> Y. Jiang,<sup>†</sup> Y. Pan,<sup>\*,†</sup> and A. L. Yarin<sup>\*,†</sup>

<sup>†</sup>Department of Mechanical and Industrial Engineering, University of Illinois at Chicago, 842 W. Taylor Street, Chicago, Illinois 60607-7022, United States

<sup>‡</sup>High-Voltage Laboratories, Technische Universität Darmstadt, Fraunhoferstr. 4, Darmstadt 64283, Germany

### Supporting Information



**ABSTRACT:** Here, we investigate the feasibility and effectiveness of electrowetting in the motion control of droplets of different liquids, which are widely used as inks in direct writing (DW)-based three-dimensional (3D) printing processes for various applications. To control the movement of DW ink droplets on dielectric substrates, the electrodes were embedded in the substrate. It is demonstrated that droplets of pure liquid inks, aqueous polymer solution inks, and carbon fiber suspension inks can be moved on multi-angled surfaces. Also, experimental results reveal that droplets of a commercial hydrogel, agar–agar, alginate, xanthan gum, and gum arabic can be moved by electrowetting. Droplets of sizes 200  $\mu\text{m}$ –3 mm were manipulated and moved by the electric field on different dielectric substrates accurately and repeatedly. Effective electrowetting-based control and movement of droplets were observed on horizontal, vertical, and even inverted substrates. These findings imply the feasibility and potential application of electrowetting as a flexible, rapid, and new method for ink droplet control in 3D printing processes.

## INTRODUCTION

**Challenges and Motivation of Ink Droplet Control in Direct Writing.** Direct writing (DW) is a class of additive manufacturing [AM, also known as three-dimensional (3D) printing] techniques which deposit functional and/or structural liquid materials onto a substrate in digitally defined locations.<sup>1–3</sup> On the basis of the dispensing form, DW can be classified into droplet-based and filament-based. DW differs from conventional AM in terms of the following characteristics. (i) The range of materials deposited can include liquid polymers,<sup>4–7</sup> particle suspensions,<sup>8–10</sup> electronically and optically functional liquids,<sup>11–14</sup> and biological liquids;<sup>15–17</sup> (ii) the track width ranges from submicrons to millimeters; and (iii) the substrate is an integral part of the final product, and it could be flat, curvilinear, round, flexible, irregular, or inflatable.<sup>3</sup> A wide variety of applications from flexible electronics fabrication to functional tissue printing have been demonstrated during the past 20 years.<sup>4–17</sup>

However, despite this progress, many grand challenges still exist in the printing quality. Ink droplet wetting and spreading coupled with the complex fluid dynamics involved have an important role in defining the surface roughness and geometrical accuracy of the features fabricated by DW.<sup>18–31</sup> Because of this complexity, many manufacturing defects,

including the coffee-ring effect, bulging, liquid puddles, liquid splashing, and scalloped or discontinued line, are caused by the undesirable wetting and movement of liquid ink on the substrate.<sup>18–31</sup>

Some research efforts have been directed on controlling the substrate wettability and hence the liquid ink droplet movement and location on the substrate to improve the print quality (e.g., eliminating the coffee-ring effect, improving the surface finish, and edge sharpness).<sup>7,32,33</sup> Controlling the ink droplet movement during the DW process would enhance the locating precision, printable feature size, and printed geometry accuracy.<sup>34–42</sup> However, all efforts that have been made to control ink droplet wetting and movement on substrates were focused on substrate surface modification, including changing the substrate chemical composition by coating a new layer or changing the surface topology.<sup>20,22–24</sup> Yet, chemical modification sometimes is undesirable as it affects the functionality and properties of the final product. The surface topology modification methods, including plasma treatment and surface machining, are time-consuming and

**Received:** April 12, 2019

**Revised:** July 18, 2019

**Published:** July 25, 2019

costly, and the modified substrate surfaces may easily get damaged during the DW process. Furthermore, the effects of these methods on droplet–substrate interaction are irreversible. Lastly and most importantly, all these control methods cannot dynamically and locally control the droplets. Lack of these capabilities significantly limits the choice of inks and DW performance.<sup>43–46</sup>

To seek information pertaining to present-day challenges and potentially inspire new techniques in an expanding industry, a new ink droplet control method using electro-wetting (EW) is proposed and explored here. Experiments were intended, designed, and performed to study the feasibility of using EW to dynamically control local wetting, spreading, and movement of DW ink droplets on a wide range of substrates.

**DW Inks.** DW techniques have been applied in industry to fabricate multiple objects for various applications employing numerous liquids as feedstock when printing. In this study, seven categories of liquid inks commonly used in DW are investigated:

**Electrically Conductive Nanofiber-Suspension Inks.** In this category, a widely used DW ink is carbon nanotube (CNT) suspension because of the light weight and excellent mechanical properties of C.<sup>8</sup> In addition, CNT suspensions are also widely used as inks for printing of energy-storage devices, such as supercapacitors and batteries, because of their excellent conductivity, large surface area, and good mechanical properties.<sup>9,10</sup> Hence, in this work, a CNT suspension ink was prepared and studied to elucidate the associated EW effects.

**Aqueous Polymer Inks.** They are often used as enhanced electrolyte materials in DW of various electrochemical devices and high-performance solid-state batteries because of their superior mechanical strength, biocompatibility, electrochemical stability, and abrasion resistance. Accordingly, in this study, aqueous polymer solutions including polyvinyl alcohol (PVA), polyethylene oxide (PEO), polyacrylamide (PAM), and polycaprolactone (PCL) are investigated.

**Nonaqueous Polymeric Liquid Inks.** Nonaqueous polymeric liquid inks are widely used in DW. This study explored three nonaqueous polymeric liquid inks: Spot-E (Spot-A Materials, Spain), trimethylolpropane triacrylate (TMPTA), and dioctyl terephthalate (DOTP). Spot-E is a photopolymerizable resin used for DW of objects for applications requiring rubbery and soft, yet resilient materials.<sup>47–50</sup> TMPTA is widely used as a functional monomer in preparing inks for DW because of its low volatility and fast cure response.<sup>51–53</sup> DOTP is usually used as a plasticizer or an additive to prepare inks for DW of objects such as phantoms for biomedical applications.<sup>54,55</sup>

**Hydrogels.** Natural ingredients such as alginate, chitosan, xanthan gum, or gum arabic are widely used for preparing water-based inks for DW-based 3D bioprinting applications such as tissue engineering and 3D food printing.<sup>56–59</sup> In this study, several natural hydrogels are prepared and investigated.

**Silicone-Based Soft Elastomers.** They are commonly used as DW inks to print fundamental construction supports in many reported electronic and soft robotic applications.<sup>60,61</sup> This type of ink also provides efficient biocompatibility for skin sensors. Two elastomers, Ecoflex and polydimethylsiloxane (PDMS), are investigated in this study.

**Ionic Liquids.** This type of ink has been employed in DW for printing batteries and other storage devices.<sup>62</sup> In addition, ionic liquids have been explored as solvents for polymerization

processes and for structures of grafted components emerging in DW-based 3D printing applications.<sup>63</sup> Benzyltrimethyl OH and NaCl ionic liquid inks are investigated in this work.

**Liquid Crystal Inks.** They have found successful applications in watches and flat-panel displays. Newer applications are being developed and used in optics, nano-manipulation, composites, and biotechnology.<sup>64</sup> Specifically, molecularly oriented liquid-crystalline polymers have shown great promise by outperforming 3D-printed polymers via creating highly ordered structures. Hence, a liquid crystal ink, 4'-pentyl-4-biphenylcarbonitrile, is investigated in this study.

**EW on Dielectrics.** Electric fields have an impact on droplets containing ionic conductors, and this phenomenon is called EW. While the term EW originated relatively recently, using surface charges to manipulate water droplets has been in practice for over a hundred years. Because of several modern applications, such as digital lenses and circuitry, atomization, spray painting, coating, aging of high voltage insulators, and so forth, interest in EW has exploded in recent years.<sup>65–68</sup> The term EW describes a droplet's ability to change its contact angle with the underlying surface when subjected to an electric field, thus changing the wettability by electrical means. Essentially, EW is an active control method, which allows switching between wettable and non-wettable surface states without modifying the surface or changing any liquid properties. EW is very repeatable and nondestructive, which is attractive for practical applications such as spray coating, spray painting, adhesion, microfluidics, and so forth.<sup>69–72</sup>

In general, two types of EW are recognized and distinguished, specifically, classical EW and EW on dielectrics (EWOD). In the case of classical EW, a droplet is in direct contact with one electrode and is separated from the second electrode by a dielectric layer. Depending on the droplet's electrical conductivity, the droplet can also be considered as an extension of the electrode. Monographs and reviews discussing EW are available from several sources.<sup>70,73</sup> In particular, the review<sup>73</sup> discusses and compares EW phenomena for a number of liquids with different dielectric properties, polarizabilities, and viscosities. One of the interesting applications is the so-called “beating mercury heart,” in which periodic EW can be realized, accompanied by a periodic change of the droplet shape or even motion on inclined surfaces.<sup>73–76</sup>

In contrast, in the EWOD applications, droplets are not in direct contact with either of the electrodes and are completely separated by a dielectric layer and an air gap. Both methods affect the equilibrium contact angle of droplets.<sup>70,77</sup> However, it should be emphasized that the voltage required to change the contact angle is lower in the case of classical EW compared to EWOD.<sup>71</sup> An increase in surface wettability requires an external work to be done, enabling the liquid to increase its free surface area and thus the free surface energy. In both cases of EW, the electric field does the external work and can be actively controlled. Generally, when a voltage is applied, EW is associated with the reduction in the solid–liquid interfacial energy. This phenomenon is due to the free charges (ions) rearranging within the liquid (implied to be an ionic conductor), consequently redistributing the forces acting between a droplet and the dielectric surface. Manipulation of these forces through EW can be observed and characterized through the changing equilibrium contact angles and is described using the Young–Lippmann equation.<sup>70</sup> Experimentally, the equilibrium contact angle can vary with the applied voltage and change from large values (hydrophobic or

even superhydrophobic) to small values (hydrophilic).<sup>78</sup> In addition, controlling the surface wettability by manipulating the electric field holds great promise for droplet manipulation in applications such as digital microfluidics,<sup>79</sup> electronic displays,<sup>80</sup> paint drying,<sup>81</sup> responsive cooling,<sup>82</sup> adjustable focusing lenses,<sup>83</sup> and so on.<sup>84,85</sup> Although EW has already proven its importance in many fields, it remains a complex phenomenon and is far from being completely understood. This lack of understanding is especially true for problems with coupled physics, for example, the interaction of droplets on a surface (DIW Printing) within an electric field, which leaves many open questions.

In the past, many researchers investigated the impact behavior of droplets onto a dry surface without an electric field. These experiments were conducted with changing surface materials and textures, which revealed a dependence of the droplet behavior on the wettability and roughness of the substrate. The impact of droplets onto a dry wall was characterized, and regimes such as deposition, prompt splash, corona splash, receding break-up, partial rebound, and complete rebound were distinguished.<sup>86</sup> Accordingly, the behavior of impacting droplets is rather complex even without an applied electric field and depends on different parameters, such as the droplet size, impact characteristics, and the Weber number as well as the surface properties.<sup>87,88</sup> The dependence on the surface properties is expressed via the values of advancing and receding contact angles,  $\theta_{adv}$  and  $\theta_{rec}$ , respectively. It was also shown that the droplet behavior can be significantly influenced by the electric field, diminishing the influence of surface properties.<sup>71</sup> Generating a net force acting on a liquid near the contact line (CL), the electric field can prevent droplet bouncing on a hydrophobic surface and induce movement of sessile droplets. This movement arises when the force applied by the electric field reduces the advancing contact angle. Depending on the receding contact angle, residual droplets can also be formed.

In the present work, the effects of electric field on 3D-printable ink droplets deposited on dielectric surfaces are investigated. The manipulation of droplet position on the surface and the elucidation of the interplay between the electric field and the droplet motion are in focus in this work. The underlying physics of EWOD is outlined, and an experimental investigation of printable inks is performed on different hydrophobic surfaces under varying conditions of EW. Experimental setups are described, results are presented, and conclusions are drawn in the following sections.

## THEORETICAL FUNDAMENTALS

In perfect conductors with very high electric conductivities, the charge relaxation time  $\tau_C$  approaches zero (i.e., the electric charges escape immediately), whereas in perfect dielectrics,  $\tau_C$  approaches infinity as the latter possess zero conductivity. Ionic conductors (electrolytes) are of interest here. They possess finite electric conductivities which correspond to finite values of the charge relaxation time. An assortment of polar and nonpolar liquids reveals the values of the charge relaxation time  $\tau_C$  in the 1  $\mu$ s to 20 s range.<sup>89</sup>

Flowing electrolytes can be affected by the electric field imposed by solid surfaces, which might be dielectric or conducting. Any flow possesses its own characteristic hydrodynamic time  $\tau_H$ , which may be associated with either the residence time of material elements in the flow zone or the

time of droplet spreading over a surface. Accordingly, the dimensionless group<sup>90</sup>

$$\alpha = \frac{\tau_C}{\tau_H} \quad (1)$$

determines the electrolyte behavior. If  $\alpha \ll 1$ , the electrolyte behaves as a perfect conductor irrespective of its relatively low conductivity. This means that the electric charge can immediately escape into a conducting wall or adjust itself to the  $\zeta$ -potential of a dielectric surface in contact. For example, a charged oil droplet of very low conductivity located at a dielectric wall for a sufficiently long time would essentially possess the characteristic hydrodynamic time  $\tau_H = \infty$ . Thus, in this case,  $\alpha = 0$ ; so the electric charges (ions) always have enough time to adjust themselves to the  $\zeta$ -potential of the underlying wall. Therefore, even a poorly conducting oil droplet can be considered as a perfect conductor in such cases. On the other hand, when a charged oil droplet impinges onto a wall and spreads after the impact on the order of time  $\tau_H = 1$  ms, the value of  $\alpha = 2 \times 10^4$  because the charge relaxation time  $\tau_C$  is about 20 s. As a result, in such a transient situation, the same oil droplet would behave as a perfect dielectric, and the prediction of the charge redistribution over its bottom during the spreading stage would require the solution of the electrokinetic equations coupled with the flow equations. Also, when  $\alpha$  is of the order of 1, the charge redistribution would happen during the flow and would be coupled with the flow evolution.<sup>91</sup>

It should be emphasized that the ion distribution at the droplet bottom could be quasi-static, which implies that it is achieved at the droplet bottom at any configuration without a delay. This assumption is true for water droplet impact, where  $\tau_C \sim 1 \mu$ s, that is, much less than the characteristic impact time  $\tau_H \sim 1$  ms, which corresponds to the case of  $\alpha \ll 1$ . This assumption would be inappropriate in cases with  $\alpha \sim 1$  and  $\alpha \gg 1$ .

In general, the electrostatic energy embedded in the droplet bottom associated with the accumulated ions is

$$E_{el} = \frac{1}{2} \int_{\text{bottom}} \sigma_{ion} U \, dS \quad (2)$$

The potential  $U$  is essentially imposed by the surface to accumulate ions in a liquid. The surface concentration of the free ions  $\sigma_{ion}$  should be found using a solution of the Laplace equation in the dielectric substrate and the electrostatic boundary conditions at its surface. Note that in the case of a conductive substrate,  $U$  is a given constant because such a substrate is equipotential.

In order to specifically find  $\sigma_{ion}$  in a droplet evolving during the impact or movement, the following electrokinetic equations should be solved:

(i) The balance equations for the cations and anions concentrations  $c^\pm$

$$\frac{\partial c^\pm}{\partial t} + \nabla \cdot (c^\pm \mathbf{v}) = D \nabla^2 c^\pm \pm \frac{De}{k_B T} \nabla \cdot (c^\pm \nabla \varphi) \quad (3)$$

They account for diffusion ( $D$  is the diffusion coefficient), convection ( $\mathbf{v}$  is the velocity field), and electric migration (with  $e$  being the proton charge,  $k_B$  being the Boltzmann's constant, and  $T$  being temperature);

(ii) The Poisson equation, which determines distribution of the electric potential  $\varphi$  in the droplet on the surface

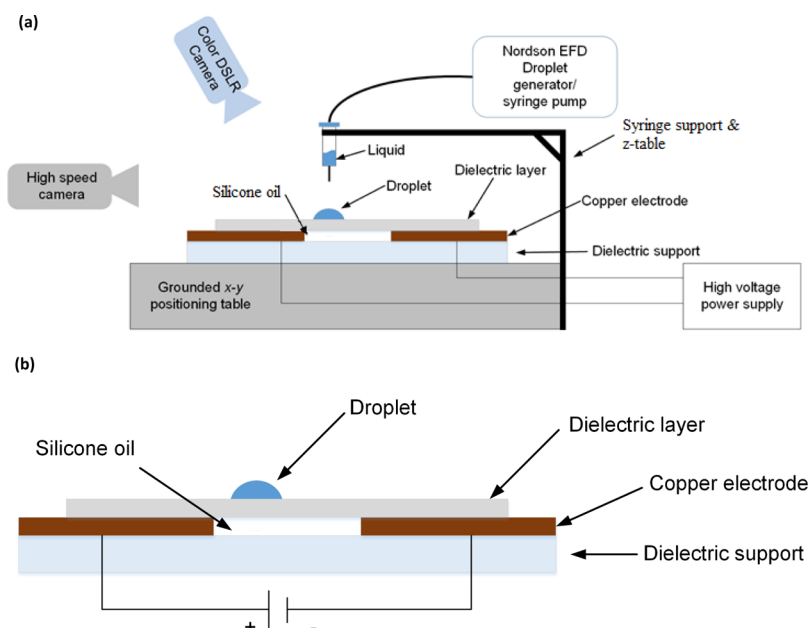


**Figure 1.** (a) Schematic of the experimental setup. (b) Details of droplet deposition and polarity.

$$\nabla^2 \varphi = -\frac{4\pi q}{\epsilon} \quad (4)$$

with  $\epsilon$  being the dielectric permittivity of liquid and the local volumetric charge equal to  $q = e(c^+ - c^-)$ . Note also that each droplet carries both anions and cations, which might be in balance if it is uncharged or unbalanced if it is charged.

(iii) The Navier–Stokes equations, which are solved to determine the velocity field  $\mathbf{v}$  affected by Coloumb force, determined using eqs 3 and 4.

The contact angle is required to find the CL velocity and thus update the drop footprint during the numerical simulations based on eqs 2–4. The contact angle should be calculated as follows. The surface tension (surface energy) at the solid–liquid interface (the droplet bottom)  $\sigma_{sl}$  is diminished from its original value  $\sigma_{sl}^0$  (without the electric field) by the value of the electric energy. This is mainly due to the presence of ions and the fact that they repel each other

$$\sigma_{sl} = \sigma_{sl}^0 - E_{el} \quad (5)$$

In equilibrium, the Young equation reads

$$\sigma_{sa} = \sigma_{sl} + \sigma_{la} \cos \theta_{eV} \quad (6)$$

where  $\sigma_{la} = \gamma$  is the surface tension,  $\theta_{eV}$  is the equilibrium contact angle after a voltage has been applied, and  $\sigma_{sa}$  is the surface tension (surface energy) at the solid–air interface.

Similarly, without voltage

$$\sigma_{sa} = \sigma_{sl}^0 + \sigma_{la} \cos \theta_{e0} \quad (7)$$

where  $\theta_{e0}$  is the known equilibrium contact angle without voltage.

Then, eqs 5–7 yield

$$\cos \theta_{eV} = \cos \theta_{e0} + \frac{E_{el}}{\gamma} \quad (8)$$

which is essentially a novel generalized form of the Young–Lippmann equation.

In the case of a rough surface, similarly, the adoption of the Wenzel-state assumption would transform eq 8 to the following form

$$\cos \theta_{eV} = r \left( \cos \theta_{e0} + \frac{E_{el}}{\gamma} \right) \quad (9)$$

where the known factor  $r$  expresses the ratio of the actual surface area of the droplet bottom to the projected one.

After the equilibrium contact angle under an applied voltage is established using eq 8 or 9, the Hoffman–Voinov–Tanner law<sup>92</sup> is utilized to find the velocity of the CL motion. Namely, the relation of the dimensionless velocity of the CL in the form of the capillary number  $Ca = u_{CL}\mu/\gamma$  (with  $u_{CL}$  being the CL velocity) and the contact angle is found as

$$Ca = g_{\text{Hoff}}(\theta_D) - g_{\text{Hoff}}(\theta_{eV}) \quad (10)$$

In eq 10,  $\theta_D$  is the dynamic advancing contact angle known at each time step from the predicted current droplet shape and

$$g_{\text{Hoff}}(x) = f_{\text{Hoff}}^{-1}(x),$$

$$f_{\text{Hoff}}(x) = \arccos \left\{ 1 - 2 \tanh \left[ 5.16 \left( \frac{x}{1 + 1.31x^{0.99}} \right)^{0.706} \right] \right\} \quad (11)$$

Note that in eq 11,  $x$  is a dummy variable.

Note also that the standard form of the Young–Lippmann eq 8 is written as<sup>70,71</sup>

$$\cos \theta_{eV} = \cos \theta_{e0} + \frac{C_s U^2}{2\gamma} \quad (12)$$

where  $C_s$  is the capacitance corresponding to a particular geometry.

The implementation of the algorithm based on the numerical solution of eqs 2–4 and 8–11 would require the solution of the 3D transient problem with the free surface and a moving CL, which is outside the scope of the present work.

Note also that an alternative approach to modeling of symmetric droplet movement on polarized and nonpolarized

dielectric surfaces and the subsequent spreading and oscillations employed the Cahn–Hilliard–Navier–Stokes technique to describe EWOD phenomena and shed light on droplet manipulations that can be used in novel applications.<sup>93</sup>

### EW-ASSISTED DW EXPERIMENTAL SETUP

To explore the EW effects acting on ink droplets in DW, we integrated an electric field generation unit into a DW prototype. As illustrated in Figure 1a, the experimental setup consists of a movable  $x$ - and  $y$ -table as a support for the specimens, along with two different droplet generation systems and a high-voltage power supply. The high voltage is selectively applied to different electrodes via a microcontroller and circuitry. To generate droplets with diameter of the order of a millimeter, an automated syringe pump (single syringe pump NE-300) is connected to a needle of appropriate size. A liquid ink droplet is pumped through the needle. The droplet size is defined by the needle diameter and the surface tension of the fluid because the droplet detaches from the needle because of gravity. The droplet diameter  $d$ , in this case, is of the order of a millimeter and varies with the needle diameters. To generate droplets with sizes smaller than 1 mm, a commercial droplet generator (Nordson Ultimus I) was used in the DW testbed. Droplets of diameter  $\sim 250 \mu\text{m}$  were generated and explored in this work. The droplet generator creates a well-defined pressure pulse for a specific time interval and forces the liquid to flow through the needle. In this case, the distance between the surface and the needle should be in the same order as the needle diameter to ensure droplet detachment.

The distance between the needle and the surface was kept small,  $h = \sim 300 \mu\text{m}$  to 3 mm, so that droplets could be deposited at specific locations above or between the electrodes. The surface on which droplets were deposited consisted of three different layers: a dielectric support layer, a copper electrode layer, and a dielectric layer, as shown in Figure 1b. Two electrodes made of a commercial copper tape were adhered to a dielectric support. Glass, polyvinyl chloride, and circuit boards were used to support the dielectric layers. The distance between the electrodes was varied between 0.127 and 25 mm to investigate its influence. The electrode–electrode distances, 0.127 and 0.15 mm, were achieved through the fabrication of self-designed circuit boards. For example, a self-designed circuit board with a pad size of 3 mm and an air insulation gap of 0.15 mm between the electrode pads is shown in Figure 2. It should be emphasized that this air gap is filled with a 5 cSt silicone oil, which is deposited as a thin coating.

A voltage between 0 and 10 kV was applied between the electrodes depending on the electrode size as well as the insulation gap. High voltages up to 10 kV are only applied for large insulation gaps like 25 mm. A reduced insulation gap requires lower voltages. This results in a driving voltage between 200 and 400 V required to move droplets with insulation gaps around 0.5 mm. Reducing the insulation gap increases the electric field strength for a constant voltage; therefore, the voltage can be reduced for small gaps while keeping the electric field strength constant. To insulate the electrodes from the liquid and to prevent short circuit, a dielectric layer is used to cover them. Accordingly, droplets are only in contact with the dielectric layer.

While initial experiments on droplet motion started with just two crudely made electrodes, printed circuit board (PCB) technologies quickly enhanced the capabilities, allowing many electrodes to be placed on the same circuit board in a small area (cf. Figure 2). Precision control of these electrodes was achieved using an Arduino Mega 2560 microcontroller coupled with an in-house developed code. By switching the polarity of the electrodes, the electric field lines and the forces associated with them were choreographed. This allowed a user-defined timing and control of droplet motion in the  $x$ -,  $y$ -, and even  $z$ -directions. A high-voltage power source was applied to high-voltage relays, which were in turn activated by a system of optocouplers and transistors used to isolate the high-voltage circuit from the Arduino microcontroller. As the polarity is switched throughout the array of electrodes, relays activate on the Arduino microcontroller's command, providing a closed circuit between the

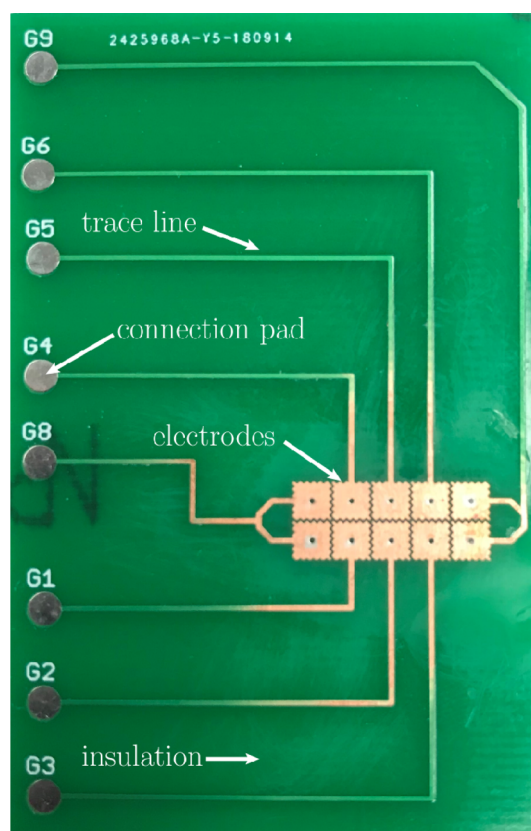


**Figure 2.** Image of an electrode array on PCB with the electrode size of 3 mm and an insulation distance of 0.15 mm. The insulation layer is invisible in this image.

electrode and high-voltage source. To deactivate the active electrode and return it to a grounded state, the relay is opened by Arduino's programming, which allows the small capacitance stored in the electrode to be neutralized by the ground via an appropriately sized high-voltage resistor. Changing the resistance controls the characteristic time required to return the electrode to a grounded state. For potential differences on the order of 100 V, 1 M $\Omega$  resistors were used, whereas 100 M $\Omega$  resistors were used to neutralize the electrodes down from voltages  $\sim 10\,000$  V. Precise droplet control was achieved through these methods, and the droplet's evolution and motion were captured using a high-speed camera (Phantom V210) and shadowgraphy. All experiments were performed under ambient conditions.

**Preparation of DW Substrates for EW Experiments.** Various dielectric substrates commonly used in DW processes are explored in this study, including commercial Teflon tape, commercial wax paper (parafilm), Teflon FEP, and PFA foil as well as commercial Kapton tape with sizes of about 25 mm  $\times$  25 mm. These substrate materials possess different surface properties including roughness, wettability, and uniformity. Unstretched Teflon tape has a hydrophobic surface with a contact angle of about 100°. To increase the hydrophobicity, the Teflon tape is stretched, which results in the contact angles of 150°. In contrast, the wax paper and Kapton tape are less hydrophobic with contact angles around 105° and 95°, respectively. In addition to different surface wettabilities, the tested dielectric layer materials also have different relative dielectric permittivity values and thicknesses, as listed in Table 1. The thickness of the dielectric layer was kept as small as possible to reduce the necessary voltage required to manipulate the droplets. The most promising dielectric layer for experiments conducted with water and water-based liquids was found to be commercial wax paper (parafilm). It will be discussed in greater detail in the results section. To achieve the best surface properties, the parafilm is stretched to reduce the thickness and is covered with a very

**Table 1. Material Properties of the Specimens**

material	thickness in mm	relative dielectric permittivity
Teflon tape (unstretched)	~0.1	~2.1
Teflon tape (stretched)	~0.02	~2.1
Parafilm	~0.02–0.13	~2.2
Kapton tape	~0.05	~3–4
Teflon FEP and PFA films	~0.005	~2.0

thin layer of silicone oil. As a result, the surface repels water very well and enables easy motion of droplets on the surface. Furthermore, the thin layer does have a negligible influence on the required voltage. When testing nonaqueous liquids, FEP was found to exhibit the best surface properties for drop motion.

**Preparation of DW Inks for EW Experiments.** To investigate the influence of ink properties on EW-based droplet control, various liquid inks were prepared, each having a unique viscosity, surface tension, and chemical composition. The tested liquid inks include aqueous polymer solutions, nonaqueous polymer solutions, hydrogels, silicone-based inks, electrically conductive inks, ionic liquids, and liquid crystals, as listed in Table 2.

**Table 2. List of Inks and Their Solubility in Water**

ink	classification	solubility in water
deionized water	common liquid	yes
50 wt % water/glycerol mix	common liquid	yes
pure glycerol	common liquid	no
CNT	nanofiber suspension	water-based suspension
basic PVA	aqueous polymeric	yes
PVA with LiCl	aqueous polymeric	yes
PVA with HCL or NaOH	aqueous polymeric	yes
basic PEO	aqueous polymeric	yes
PEO with LiCl or KCl	aqueous polymeric	yes
PAM	aqueous polymeric	yes
PCL	aqueous polymeric	yes
Spot-E	non-aqueous polymeric	no
DOTP	non-aqueous polymeric	no
TMPTA	non-aqueous polymeric	no
Ecoflex	silicone-based	no
PDMS	silicone-based	no
commercial hydrogel	hydrogel	yes
agar-agar	hydrogel	yes
alginate	hydrogel	yes
xanthan gum	hydrogel	yes
gum arabic	hydrogel	yes
chitosan	hydrogel	yes, with acid
sericin	hydrogel	yes
benzyltrimethyl OH in water	ionic liquid	yes
benzyltrimethyl OH in methanol	ionic liquid	yes
NaCl in water	ionic liquid	yes
4'-pentyl-4-biphenylcarbonitrile	liquid crystal	no

**Reference Liquid.** As a reference, pure deionized water is tested, which has a surface tension of  $\gamma = 72.75 \times 10^{-3}$  N/m and a kinematic viscosity of  $\nu = 1.0034 \times 10^{-6}$  m<sup>2</sup>/s under ambient conditions. To vary the viscosity and surface tension, deionized water was mixed with pure glycerol, which has a surface tension of  $\gamma = 63.4 \times 10^{-3}$  N/m and a kinematic viscosity of  $\nu = 5.2 \times 10^{-5}$  m<sup>2</sup>/s. A mixture of 50% water and 50% glycerol was tested along with pure glycerol.

**Electrically Conductive Nanofiber-Suspension Ink.** Multiwalled CNTs (MWCNTs) (purity > 95 wt %, 10–20 nm) were purchased

from Cheaptubes (product code 030103) and used as received. MWCNTs (50 mg) and 125 mg of sodium dodecyl sulfate powder (>99.0%, Sigma-Aldrich) were mixed with 50 mL of deionized water in a mixer (AR-100, Thinky) at 2000 rpm for 15 min and then sonicated in a probe sonicator (QSonica Q500, 60% power) for 1 h. After that, the CNTs were uniformly dispersed in the suspension. The prepared water-based nanotube ink is a conducting fluid due to the presence of the suspended CNTs. The rheological behavior of the CNT ink is similar to that of water, but the electrical conductivity is much higher. A droplet of a CNT ink was placed on a glass specimen and dried at ambient temperature. The orientation of the CNTs was investigated by scanning electron microscopy (SEM) after drying, with and without the influence of an electric field. Figure 3 shows an

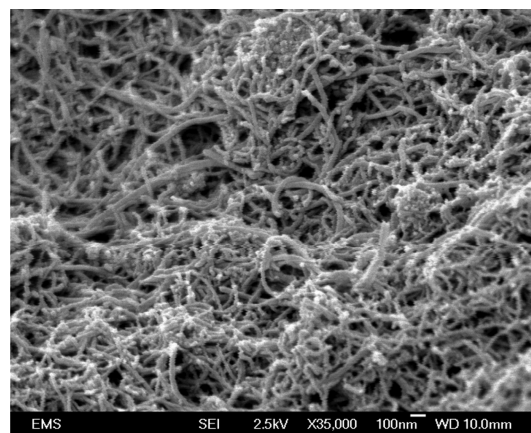


**Figure 3.** SEM image of the sonicated ink (a CNT suspension) dried under the effect of 1 kV electric potential difference at an ambient temperature.

example of the CNTs observed in a SEM image. The length of individual CNTs is of the order of several microns, and the diameter is less than 100 nm. The CNTs are randomly distributed and not aligned by the electric field, implying that the electric field as well as the ink preparation process, including sonication, have no influence on the alignment and size of the CNTs in the prepared ink.

**Aqueous Polymer Solutions.** Preparation of the PVA-based electrolyte ink (PVA) is a two-part process. First, 6 g of PVA powder (Mowiol 18-88,  $M_w \sim 130\,000$  Da, Sigma-Aldrich) was added to 40 g of deionized water. Second, the solution was stirred (Eurostar 60, IKA) on an 85 °C hot plate for at least 45 min at a 500 rpm rotating speed. This base solution was kept as the control, while other components were added to the solution to check their influence on the droplet motion. PVA is a highly polar molecule with amphiphilic properties due to its hydrophilic –OH group. Lithium chloride powder (12 g, >99.0%, Sigma-Aldrich) was added to the base solution and stirred to form an electrolyte. Dissolving the lithium chloride powder adds ions in the ink and thus increases the mobility of electrons. Furthermore, the pH value of the base solution was measured at pH ~ 6. Adding some acid (HCl) or base (NaOH) resulted in a changed pH value, and in both cases, only a droplet of the acid or base was mixed with the original solution. Adding a droplet of 37% HCl solution resulted in a pH value of ~2, and the solution with a droplet of 50% NaOH solution yielded pH ~ 12.

Similar to the preparation of the PVA solution, 6 g of PEO powder (Sigma-Aldrich,  $M_w \sim 200\,000$  Da) is dissolved in 40 g of deionized water resulting in a 13% solution. After mixing, the solution is stirred on a hot plate at a temperature of 85 °C for several hours. In contrast to PVA, PEO is a nearly nonpolar molecule because of the symmetric chemical structure. Nevertheless, the base PEO solution was also mixed with salts, and the results were compared with the modified inks.

To compare the influence of the polarity between molecules, another highly polar molecule PAM was prepared using a procedure

similar to the PEO and PVA solutions. PAM (6 g, Sigma-Aldrich,  $M_w \sim 150\,000$  Da) is dissolved in 40 g of deionized water. The solution is stirred for several hours on a hot plate at a temperature of 85 °C.

Besides the above-mentioned aqueous polymer solutions, PCL solution is prepared by dissolving 3.47 g of PCL powder in 40 g of acetone, and the mixture is stirred on a hot plate at a temperature of 85 °C for several hours.

**Nonaqueous Polymeric Liquid Inks.** Spot-E liquid polymer was purchased from Spot-A Materials (Spain) and used as received. TMPTA and DOTP were purchased from Sigma-Aldrich (U.S.). Spot-E has the kinematic viscosity of  $\nu = 3.64 \times 10^{-4}$  m<sup>2</sup>/s. The purchased TMPTA and DOTP possess viscosities of  $\eta = 80$ –135 mPa s and  $\eta = 63$  mPa s at 25 °C, respectively. DOTP was used as received. TMPTA (20 mL) was mixed with 20 mL of hexane (Sigma-Aldrich) for printability and experiments.

**Hydrogels.** To explore hydrogel inks affected by the electric field, several inks were prepared in the present study. A commercially available hydrogel (Skintegrity by Medline) was purchased and mixed with water. For printability, 10 g of the hydrogel is mixed with 20 mL of deionized water to form a printable gel. In addition to the commercial hydrogel, several gels commonly used in 3D bioprinting are prepared as follows: Alginate powder (2.1 g) purchased from Sigma-Aldrich is mixed with 40 mL of deionized water. The mixture is stirred for several hours at a temperature of 85 °C until fully dissolved. In a similar manner, 7 g of gum arabic (Sigma-Aldrich) is dissolved in 40 mL of deionized water to prepare a 15 wt % solution. Two grams of sericin (Bonding Chemical) is dissolved in 8 g of deionized water forming a 20 wt % solution. Xanthan gum (Sigma-Aldrich) and agar-agar (Sigma-Aldrich) are also dissolved in deionized water and stirred on a hotplate in 0.5 and 2 wt % solutions, respectively. In contrast to the other hydrogels formed solely in deionized water, chitosan is dissolved in a mixture of formic acid and water. Chitosan requires an acidic solution to fully dissolve, so a mixture of 20 mL of deionized water and 20 mL of formic acid is used to dissolve 2.1 g of chitosan. The three ingredients are stirred on a hot plate for several hours at a temperature of 85 °C, forming a 5% wt chitosan solution.

**Silicone-Based Inks.** Two silicone-based inks commonly used in 3D printing<sup>94–97</sup> are investigated. The first silicone-based ink is prepared by mixing Ecoflex with Smooth-On at the ratio of 50:50. The second silicone-based ink, PDMS, is prepared by mixing the base and the curing agent at the ratio of 10:1. In their uncured state as used in DW, Ecoflex has a viscosity  $\eta \sim 3000$  mPa s at 25 °C, whereas the uncured PDMS has a viscosity of  $\eta = 3500$  mPa s at 25 °C.

**Ionic Liquids.** Several room-temperature ionic liquids were purchased from Sigma-Aldrich and used as received without further modification. Benzyltrimethyl hydroxide solution (40% wt in H<sub>2</sub>O) and benzyltrimethyl hydroxide (40% wt in methanol) are both tested. A third ionic liquid is formed by dissolving table salt to near saturation levels ( $\sim 26\%$  wt).

**Liquid Crystals.** The nematic liquid crystal 4'-pentyl-4-biphenyl-carbonitrile (liquid crystal, nematic, 98% Sigma-Aldrich), more commonly known as SCB, was purchased and used in the present experiments without any further modification.

**Ink Properties.** Rheological behavior of the inks is characterized in a rotational viscometer (Brookfield DV II+ Pro). Every ink prepared in this study was tested by increasing and decreasing the shear rate between 10 and 90% of the maximum torque produced by the rotational viscometer. Hence, for every shear rate, two values for the shear stress and viscosity were measured. Figures 4 and 5 show the measured flow curves of the selected inks. Figure 4 shows that xanthan gum and the hydrogel revealed clear shear-thinning behavior. Also, alginate revealed weak shear-thinning. All other liquids revealed an almost constant viscosity, that is, the Newtonian behavior in the tested shear-rate range.

In addition, the inks were tested using a uniaxial elongational rheometer based on capillary thinning of a liquid thread.<sup>98–100</sup> The uniaxial elongation tests were conducted with the commercially available ink (Spot-E), TMPTA, DOTP, and Ecoflex. The results of these tests revealed Newtonian behavior (the linear-in time decrease of the cross-sectional radius of the thread) and are not included here

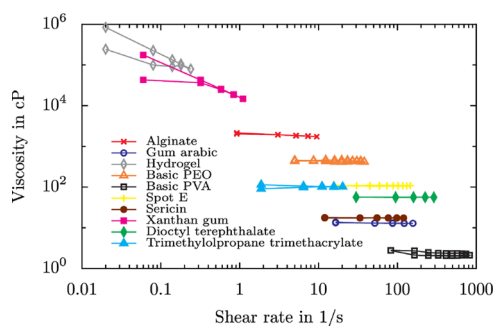


**Figure 4.** Flow curves of different inks measured using the rotational viscometer, Brookfield DV II+ Pro.

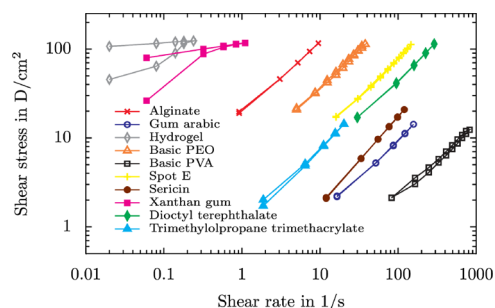


**Figure 5.** Shear stresses corresponding to the flow curves of Figure 4.

for brevity. Similarly, the test results for the photosensitive ink, which revealed Newtonian behavior in simple shear, is not detailed here for brevity. Inks which exhibit nonlinear thread thinning in time are non-Newtonian, and the corresponding results obtained using a uniaxial elongational rheometer<sup>98–100</sup> are depicted in Figure 6. The filament

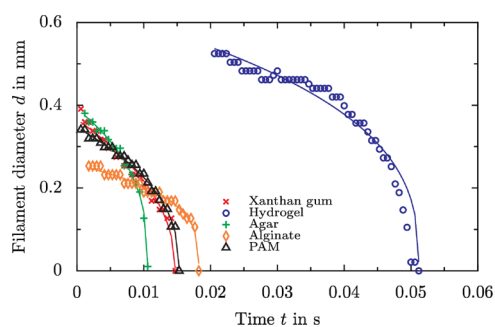


**Figure 6.** Results of the uniaxial elongation experiment, which revealed non-Newtonian behavior.

diameter formed during the experiments is measured as a function of time. Because of the surface tension-driven squeezing of liquid from the filament, its diameter decreases in time until the filament breaks up. Figure 6 shows the measured filament diameter as a function of time as well as the corresponding data fits. Thinning of filaments of inelastic non-Newtonian fluids reveals a power-law behavior corresponding to the fits in Figure 6, which are similar to those in ref 101. According to the results of the elongational experiments presented in Figure 6, xanthan gum, hydrogel, agar-agar, alginate, and PAM are shear-thinning liquids with the uniaxial elongation results being in agreement with those of the simple shear flow experiments in Figures 4 and 5.

## RESULTS AND DISCUSSION

Experiments were performed under different conditions with sessile droplets of different inks on a wide range of surfaces. Sessile droplet diameters were chosen with respect to the

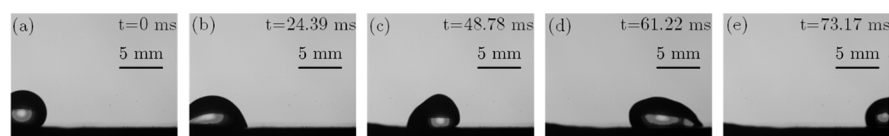


**Figure 7.** Motion of a sessile droplet from a grounded electrode (left) to the high-voltage electrode (right) accompanied by a stick-slip motion and the corresponding oscillations (surface waves on the droplet surface) at 8 kV. The interelectrode distance is 12 mm.

electrode sizes. It was found that the droplet footprint needed to commensurate to the electrode area. For example, droplets which were considerably smaller than the underlying electrode did not reveal an increased wetting in the direction of electrode switching and therefore showed no movement on the surface. In cases where droplets were significantly larger than the electrode, they were unable to be confined above the electrode, as undesirable flows and nonuniform shapes ensued. Air entrapment between the dielectric layer and the electrodes was avoided with the use of a silicone layer (shown previously in Figure 1a,b) to ensure a well-defined electric field. To test EW capability in controlling ink droplet motion on hydrophobic surfaces, different surfaces were prepared, as described previously.

**Horizontal Motion of Sessile Droplets.** To determine the best surface and surface properties for controlling sessile droplet motion of different inks, experiments were performed on unstretched and stretched Teflon as well as on stretched parafilm. For these experiments, several liquids including deionized water, pure glycerol, 50 wt % glycerol–water mixture, basic PEO solution, basic PVA solutions, and Spot-E were tested. The initial surface used to investigate droplet motion was a glass sheet with copper electrodes spaced at distances between 15 and 25 mm. Such a wide variation in electrode placement helped to determine the strength of the electric field required to move droplets over a predetermined distance.

To determine the effect of droplet placement and orientation within the electric field, ink droplets were set at different locations between the electrodes. The droplet motion was captured by a high-speed camera when the electric field was switched on. Through these experiments, the position, the droplet size, and the applied voltage have all shown significant impacts on motion.

As shown in the Supporting Information in Video 1, at low voltages, the electric field between the electrodes does not lead to droplet motion regardless of its location. The droplet may lean toward one electrode, but the three-phase CL stays pinned for low voltages. A further increase in the electric field strength causes droplets with out-of-center positions to move. Droplets with a larger volume always require a lower voltage to begin moving irrespective of the substrate surface. The larger the droplets are, the larger is the disparity between their right- and left-hand sides, if they are located off the center of the electrodes. Thus, they are subjected to a higher net pulling force. For the tested substrate surfaces, the stretched parafilm produced the most accurate and repeatable results. On the other hand, Teflon has nonuniform surface properties and thus less repeatable results. For both stretched and unstretched Teflon, no difference in the motion onset voltage was observed. Nevertheless, Teflon stretching decreased the layer thickness and may have had an influence on its hydrophobicity. It should be emphasized that a lower voltage was required in the case of the parafilm surface in comparison with that of the Teflon surface.

In most cases, the droplet motion reveals a stick-slip pattern at the CL resulting in oscillations within droplets. Variations of the contact angle cause a partial spreading of the droplet. Figure 7 shows the stick-slip motion of a water droplet and the corresponding oscillations. As shown in Supporting Information Videos 2 and 3, with an increased liquid viscosity, droplets were observed to creep on the surface, which resulted in a smoother motion. Under low electric field strengths, droplets located at the center between two electrodes are merely deformed and reveal no motion. In contrast, high electric field strengths induce motion of all droplets, irrespective of their positions.

Besides the initial placement, it was also found that sessile droplet motion depends on the electrode configuration. Uncharged droplets usually move to the high-voltage electrode and, therefore, away from the low-voltage electrode, as shown in Figure 7. However, in some cases, opposite direction of droplet motion was observed, most probably because of a net charge on the droplet, which causes an additional Coulomb force. Depending on the electric field strength, this additional force can cause motion in the opposite direction, as observed. The origin of the net charge might be in the accumulated charges on the dielectric layer, which are transferred to the droplet, or in charges, which are transferred during droplet deposition.<sup>71,102,103</sup>

For a more controlled droplet motion, an electrode array was designed, as shown in Figure 2. The electrodes are covered with a stretched parafilm and a thin layer of silicone oil (10 cSt), which increased the ability of droplets to move. In addition, the silicone oil ensures that no air is entrapped between the electrodes and the dielectric layer. The size of the electrodes shown in Figure 2 is 3 mm × 3 mm, and the distance between the electrodes is 0.15 mm. Hence, droplets can be moved within a very short distance and very precisely. If a droplet needs to be moved for a long distance, an electrode array similar to that in Figure 2 is to be used. Because of the small insulation gaps between the electrodes as in Figure 2, droplet motion is possible even at low voltages such as ~200 V. It should be emphasized that the voltage required to trigger droplet motion decreases with a decrease in the interelectrode distance. The smaller the electrodes and the interelectrode distance, the lower is the required voltage to achieve the critical electric field strength for triggering the droplet motion. With the electrode array as shown in Figure 2, repeatable drop motions can be performed at different speeds, with switching at frequencies of ~10 Hz. Besides the simple linear movement, the arrays were also programmed allowing precise control in two orthogonal directions. To manipulate ink droplets with smaller sizes, electrode sizes are reduced to about 0.127 mm, and the interelectrode distance is also reduced to 0.090 mm. Similar results were observed with this smaller electrode array, cf. Supporting Information, Video 4.

However, it should be emphasized that controlled droplet motion was impossible for all liquids studied. Definite and precise motion control was achieved for most of the aqueous

solutions including pure water and CNT suspensions, which behave like water. Table 3 summarizes the observed outcomes related to the motion for the liquids investigated in these experiments.

**Table 3. Summary of the Tested Liquids and the Resulting Outcomes Related to Droplet Motion**

liquid	classification	moveable
deionized water	common liquid	yes
pure glycerol	common liquid	no
50 wt % water–glycerol mix	common liquid	yes
CNT	nanofiber suspension	yes
basic PVA	aqueous polymeric	no
PVA with LiCl	aqueous polymeric	no
PVA with HCl or NaOH	aqueous polymeric	no
basic PEO	aqueous polymeric	yes
PEO with LiCl or KCl	aqueous polymeric	yes
PAM	aqueous polymeric	yes
PCL	aqueous polymeric	no
Ecoflex	silicone based	yes
PDMS	silicone based	no
hydrogel	hydrogel	yes, if diluted with water
agar–agar	hydrogel	yes
alginate	hydrogel	yes
xanthan gum	hydrogel	yes
gum arabic	hydrogel	yes
chitosan	hydrogel	no
sericin	hydrogel	yes
Spot-E	non-aqueous polymeric	(yes) limited
DOTP	non-aqueous polymeric	yes
TMPTA	non-aqueous polymeric	yes, if diluted with hexane
benzyltrimethyl OH in water	ionic liquid	yes
benzyltrimethyl OH in methanol	ionic liquid	(yes) limited
NaCl in water	ionic liquid	yes
4'-pentyl-4-biphenylcarbonitrile	liquid crystal	(yes) limited

As shown in Supporting Information Video 5, droplets of aqueous solutions of PVA and nonaqueous Spot-E ink revealed a reduced or very random and uncontrollable motion: typically, they are stuck at the surfaces and left residuals near the CL. PVA is a highly polar amphiphilic molecule, which could cause such observed behavior even though being in aqueous solution. In contrast, droplets of aqueous solutions of PEO or PAM could be moved very precisely. PEO is an almost nonpolar molecule, and droplets of its solutions could be

moved at several concentrations. To explore the influence of polarity of molecules on droplet behavior, PAM was also employed. PAM molecules are also polar (as PVA molecules are), but droplets of PAM solutions could still be moved by the electric field very precisely, in contrast to droplets of PVA solutions. It can be concluded that polarity of PVA molecules is not the reason that PVA solution droplets cannot be controlled, albeit the exact reason is currently unknown.

As summarized in Table 3, most of the hydrogel droplets can be manipulated by the electric field. However, since the prepared hydrogel inks had high initial viscosities, their dilution (thinning) was required for droplet movement. After thinning, such hydrogels as alginate, agar–agar, xanthan gum, and gum arabic formed droplets that could easily be moved on the substrates. In contrast, chitosan was the only hydrogel solution, whose droplets revealed no movement in the present experiments. One explanation could be that chitosan solution contains formic acid, which was necessary to fully dissolve chitosan. Since this was the only hydrogel dissolved in the water/formic acid mixture, it is hypothesized that formic acid is responsible for the different behavior observed with droplets of the chitosan solution.

The commercially available monomers, such as DOTP and TMPTA, formed droplets that could be moved by applying the electric field. However, unlike DOTP which could be moved at the original concentration, TMPTA had to be diluted with equal parts of hexane to reduce its viscosity.

In DW 3D printing processes, droplets of sizes  $\sim 200 \mu\text{m}$  are of special interest. The movement of such droplets requires electrode arrays much smaller than the one shown in Figure 2. The smallest electrode size used in the present study was  $127 \mu\text{m} \times 127 \mu\text{m}$  (which is smaller than the one in Figure 2 by about 24 times). In the case of small electrodes and droplets on the order of  $200 \mu\text{m}$ , the motion of water and any other ink, marked as moveable in Table 3, is possible in two directions. However, droplets of Spot-E ink in the size range  $200 \mu\text{m}$  to  $3 \text{ mm}$  did not move as easy as those of water. It was assumed that motion of Spot-E is inhibited by the curing of the ink because of ambient light. Therefore, motion of the droplets consisting of Spot-E is investigated in darkness. The experiments show that the motion of the ink droplets is increased but still incomparable to the motion of water droplets. In addition to the curing of the ink, the surface properties have a large influence on the motion of the droplet. The more a surface repels a liquid, the easier the liquid moves on the surface in the electric field. The mobility of Spot-E droplets on the stretched parafilm surface is seemingly also decreased because of surface wetting properties. Changing the substrate to FEP slightly increased the mobility of Spot-E droplets, though still nowhere close to that of water droplets.

Splitting of droplets of moveable inks is observed at high electric field strengths, depending on the surface properties and droplet location. On a parafilm, droplet splitting happened at the voltage of  $\sim 5 \text{ kV}$  for droplets with diameters of  $\sim 2 \text{ mm}$

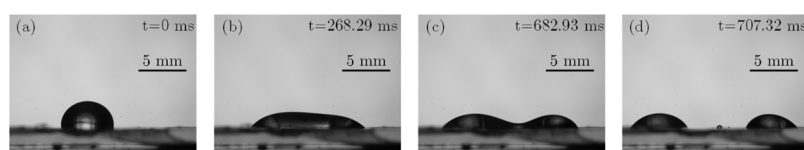


**Figure 8.** Droplet splitting with a tiny residual droplet staying in the middle. Both bigger droplets move to different electrodes.

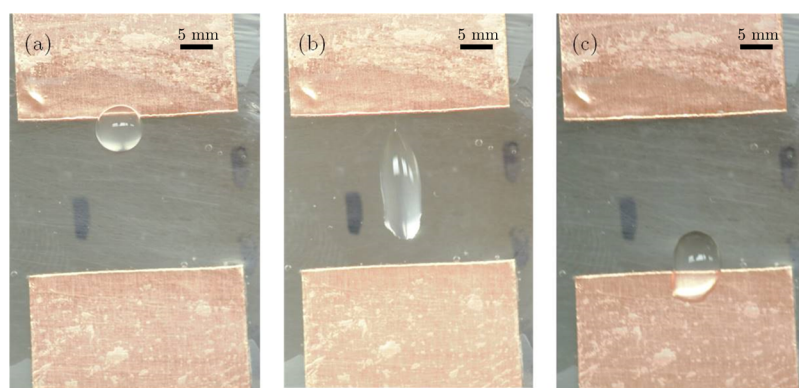


**Figure 9.** PEO droplets. (a) Original shape of the droplet (aqueous 10 wt % PEO solution; PEO  $M_w = 200\,000$  Da). (b) Deformed droplet as well as (c) the final position of the droplet. During droplet motion, it acquires a teardrop shape and forms a tail shaped like a cone.

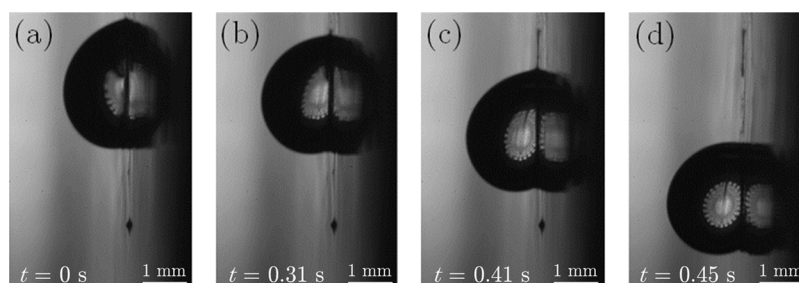


**Figure 10.** Stick and release of a water droplet on a vertical wall. Panel (a) shows the droplet stick to the wall, (b) the moment of release, and (c,d) the sliding motion of the droplet on the wall.

and the inter-electrode distance of 5 mm. The droplet size significantly influences the occurrence of droplet splitting. The larger the droplet volume, the lower the voltage resulting in droplet splitting. Nevertheless, the volume is limited by the distance between the electrodes because if the droplet touches both electrodes at the same time, a short circuit occurs. The propensity to droplet splitting is diminished at an increased voltage. In the case of droplet splitting, two droplets appear as a result. Both the resulting droplets move to one of the electrodes, and a tiny residual droplet might rest at the initial position. Figure 8 shows an example of droplet splitting with a tiny residual droplet in the middle. Droplet splitting can also be viewed in Video 6 in the Supporting Information.

In contrast to deionized water or glycerol, droplets of aqueous polymer solutions have a tearlike shape and do not move strictly toward the grounded electrode. The shape of the droplet is asymmetric relative to its longitudinal middle cross-section. In most cases, a tail is formed behind the droplet (Figure 9), which resembles tails formed by bubbles rising in aqueous polymer solutions.<sup>104</sup> This phenomenon is presumably caused by high elastic stresses (associated with the elongational viscosity) arising at the rear side of the droplet because of its propensity to pin at the surface. In contrast to the tested Newtonian liquid droplets, the motion of droplets of the aqueous polymer solutions between the electrodes is not straight anymore, but rather meandering.

#### Inclined and Vertical Motion of Sessile Droplets.

Because of the fact that droplets are typically attracted to the high-voltage electrode, the setup can also be used to hold a droplet in place, even on inclined surfaces. The electric field holds a droplet in place on inclined surfaces up to and beyond the angle of  $90^\circ$  (a vertical wall), as shown in Figure 10. Switching the electric field off results in droplet release and a

sliding motion on the surface, as shown in Video 7 in the Supporting Information. In the case of pendent droplets, the release moment is actively controlled by turning the electric field off. When being on, the electric field influences surface wetting and holds the droplet on the inverted substrates. Switching off the electric field changes the wetting angle on the surface, reducing the surface energy and allowing detachment from the inverted surface, provided the droplet is large enough for gravity to be the dominant force. Increasing the electric field strength subsequently increases the surface wettability. This pulls the droplet against gravity to the inverted surface, as shown in Figure 11. As a result, pendent droplets that would

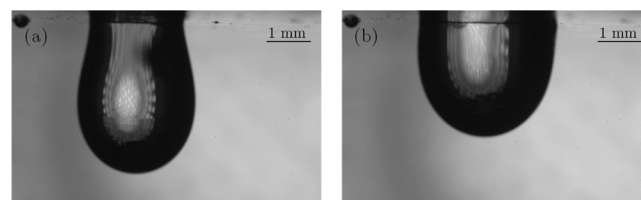


**Figure 11.** Example of a pendent droplet, which is not large enough to detach from the surface. (a) Droplet shape and contact angle without electric field and (b) enhanced surface wetting and attraction of the droplet to the surface due to the electric field.

normally detach from an inverted surface can be sustained by an electric field, giving a user-defined control over detachment. Such suspended droplets can easily be detached from the surface simply by switching the electric field off. However, it should be noted that sometimes a small residual droplet may remain attached to the surface because, with smaller droplets, surface tension remains the dominant force. A demonstration of this phenomenon is depicted in Figure 12 and shown in



**Figure 12.** Example of a pendant droplet sustained by the electric field (a). After switching the electric field off, the droplet detaches from the surface (b), and a residual droplet sticks to the surface (c).

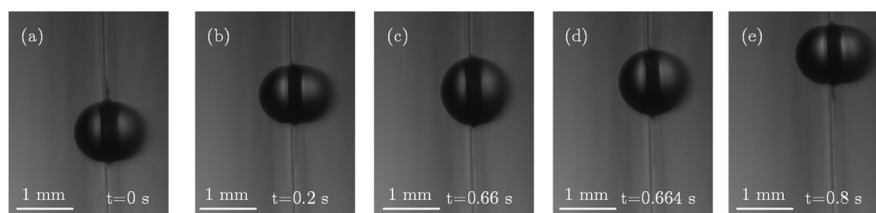


**Figure 13.** Upward motion of a water droplet with a volume of about  $0.3 \mu\text{L}$  on the parafilm and silicone oil.

**Video 8** of the Supporting Information. In addition to holding a suspended droplet with an electric field, such droplets could also be moved with the electric field. The motion of suspended droplets occurred in a manner very similar to that on a nonflipped substrate when the droplets were smaller than 1 mm. Evidence of motion of suspended droplets is presented in **Video 9** in the Supporting Information.

For smaller droplet sizes (about 1 mm, or smaller), a vertically oriented setup can be used to move droplets against the gravity force. Large droplets are too heavy and pulled down, whereas for the smaller droplets, the pulling electric force is stronger than gravity. Hence, small droplets can be moved against gravity on a vertical wall.

However, for the vertical motion of droplets, switching of the electrodes requires caution. During the switching of the electrodes, a high voltage is applied to the two electrodes to prevent a droplet from sliding down the surface due to gravity. Accordingly, the droplet is pinned to the electrode array and pulled upward as soon as the lower electrode is switched off. **Figure 13** along with **Video 10** from the Supporting Information show the upward motion of a droplet with a size of about 1 mm. As shown in the figure, the droplet moves upward in panels (a) to (b). Panels (c) to (e) in **Figure 13** show an additional upward motion of the droplet in more detail. As soon as the electric field switches from one electrode to another, the droplet is stretched as shown in panel (c). Then the droplet starts to move upward, as in panel (d), and reaches the final position, as shown in panel (e). Panels (a), (b), and (e) in **Figure 13** correspond to the end of an electrode. There, the droplet is held in place by the electric field, and its shape is almost hemispherical.

## CONCLUSIONS

The present experiments revealed that the electric field in a dielectric DW substrate can cause ink droplet motion on it depending on the droplet liquid as well as the substrate surface properties. It was shown that droplets of many aqueous polymer inks and CNT suspension inks can be moved on horizontal substrate surfaces. For example, several polymer inks, such as PEO and PAM, revealed droplet motion comparable to that of water. However, PVA ink droplets could not be moved by the electric field: the droplets were stuck to the surface and left a residual near the CL. On the other hand, PVA droplets without the electric field were not

stuck and can freely slide on the surface. PVA is a highly polar molecule as also PAM. Therefore, the difference in their behavior cannot be attributed to polarity, and the inability of PVA droplets to move is an open question.

With the exception of chitosan, all hydrogel droplets could be moved by the electric field. This includes a commercial hydrogel, agar-agar, alginate, xanthan gum, and gum arabic. The inability of chitosan droplets to move could probably be attributed to formic acid present in addition to water to dissolve chitosan.

Furthermore, droplets of several commercially available monomers, which are widely used as feedstock in DW 3D printing, can be manipulated by the electric field. In contrast, droplets of commercial products such as Spot-E are less affected by the electric field because of the curing action of light and excessive wettability of the substrate surfaces studied.

Overall, droplets with sizes between  $\sim 200 \mu\text{m}$  and 3 mm were formed from many liquids with a wide range of viscosities. These include Newtonian and non-Newtonian polymeric solutions, CNT suspensions, as well as hydrogels, which are commonly used as DW ink, can be manipulated and moved by the electric field in the dielectric substrate. This can be done with high accuracy and repeatability. The experimental findings indicate that EW is a feasible and effective method for controlling ink droplet–substrate interaction dynamically and locally in the DW 3D printing process. Future work will focus on (i) investigation of the EW effects on the DW printed trace quality and (ii) development of the novel EW-assisted DW 3D printing process.

## ASSOCIATED CONTENT

### Supporting Information

The Supporting Information is available free of charge on the ACS Publications website at DOI: [10.1021/acs.langmuir.9b01061](https://doi.org/10.1021/acs.langmuir.9b01061).

- Droplet of water showing no movement as the applied potential difference is too low (MP4)
- Stick-slip tendencies of a droplet (AVI)
- Reduced stick-slip tendencies with increased viscosity (AVI)
- Movement on a small array (MOV)
- Random movement of PVA (MOV)
- Droplet splitting (AVI)

Release from the vertical wall (AVI)  
 Controlled release of the pendent droplet (AVI)  
 Droplet movement on the inverted surface (AVI)  
 Droplet movement on the vertical surface (AVI)

## AUTHOR INFORMATION

### Corresponding Authors

\*E-mail: [ayarin@uic.edu](mailto:ayarin@uic.edu) (A.L.Y.).

\*E-mail: [yayuepan@uic.edu](mailto:yayuepan@uic.edu) (Y.P.).

### ORCID

J.-M. Löwe: 0000-0002-3863-7184

A. L. Yarin: 0000-0001-8032-2525

### Author Contributions

<sup>§</sup>Equal contribution.

### Notes

The authors declare no competing financial interest.

## ACKNOWLEDGMENTS

This material is based upon work supported by the National Science Foundation under Grant Number 1825626. Any opinions, findings, and conclusions or recommendations expressed in this material are those of the author(s) and do not necessarily reflect the views of the National Science Foundation.

## REFERENCES

- Lewis, J. A.; Gratson, G. M. Direct writing in three dimensions. *Mater. Today* **2004**, *7*, 32–39.
- Hon, K. K. B.; Li, L.; Hutchings, I. M. Direct writing technology—Advances and developments. *CIRP Ann.—Manuf. Technol.* **2008**, *57*, 601–620.
- Gibson, I.; Rosen, D.; Stucker, B. *Additive Manufacturing Technologies: 3D Printing, Rapid Prototyping, and Direct Digital Manufacturing*; Springer, 2014.
- Maynor, B. W.; Filocamo, S. F.; Grinstaff, M. W.; Liu, J. Direct-writing of polymer nanostructures: poly (thiophene) nanowires on semiconducting and insulating surfaces. *J. Am. Chem. Soc.* **2002**, *124*, 522–523.
- Sirringhaus, H.; Kawase, T.; Friend, R. H.; Shimoda, T.; Inbasekaran, M.; Wu, W.; Woo, E. P. High-resolution inkjet printing of all-polymer transistor circuits. *Science* **2000**, *290*, 2123–2126.
- de Gans, B.-J.; Duineveld, P. C.; Schubert, U. S. Inkjet printing of polymers: state of the art and future developments. *Adv. Mater.* **2004**, *16*, 203–213.
- Bharathan, J.; Yang, Y. Polymer electroluminescent devices processed by inkjet printing: I. Polymer light-emitting logo. *Appl. Phys. Lett.* **1998**, *72*, 2660–2662.
- Salvetat, J.-P.; Bonard, J.-M.; Thomson, N. H.; Kulik, A. J.; Forró, L.; Benoit, W.; Zuppiroli, L. Mechanical properties of carbon nanotubes. *Appl. Phys. A: Mater. Sci. Process.* **1999**, *69*, 255–260.
- Ahmad, S.; Copic, D.; George, C.; De Volder, M. Hierarchical assemblies of carbon nanotubes for ultraflexible Li-ion batteries. *Adv. Mater.* **2016**, *28*, 6705–6710.
- Muth, J. T.; Vogt, D. M.; Truby, R. L.; Mengüç, Y.; Kolesky, D. B.; Wood, R. J.; Lewis, J. A. Embedded 3D printing of strain sensors within highly stretchable elastomers. *Adv. Mater.* **2014**, *26*, 6307–6312.
- Ahn, B. Y.; Lorang, D. J.; Lewis, J. A. Transparent conductive grids via direct writing of silver nanoparticle inks. *Nanoscale* **2011**, *3*, 2700–2702.
- Parker, S. T.; Domachuk, P.; Amsden, J.; Bressner, J.; Lewis, J. A.; Kaplan, D. L.; Omenetto, F. G. Biocompatible silk printed optical waveguides. *Adv. Mater.* **2009**, *21*, 2411–2415.
- Gratson, G. M.; Xu, M.; Lewis, J. A. Microperiodic structures: Direct writing of three-dimensional webs. *Nature* **2004**, *428*, 386.
- Gratson, G. M.; García-Santamaría, F.; Lousse, V.; Xu, M.; Fan, S.; Lewis, J. A.; Braun, P. V. Direct-write assembly of three-dimensional photonic crystals: Conversion of polymer scaffolds to silicon hollow-woodpile structures. *Adv. Mater.* **2006**, *18*, 461–465.
- Barry, R. A.; Shepherd, R. F.; Hanson, J. N.; Nuzzo, R. G.; Wiltzius, P.; Lewis, J. A. Direct-write assembly of 3D hydrogel scaffolds for guided cell growth. *Adv. Mater.* **2009**, *21*, 2407–2410.
- Odde, D. J.; Renn, M. J. Laser-guided direct writing for applications in biotechnology. *Trends Biotechnol.* **1999**, *17*, 385–389.
- Therriault, D.; Shepherd, R. F.; White, S. R.; Lewis, J. A. Fugitive inks for Direct-Write assembly of Three-Dimensional microvascular networks. *Adv. Mater.* **2005**, *17*, 395–399.
- Chang, R.; Nam, J.; Sun, W. Effects of dispensing pressure and nozzle diameter on cell survival from solid freeform fabrication-based direct cell writing. *Tissue Eng., Part A* **2008**, *14*, 41–48.
- Xu, T.; Jin, J.; Gregory, C.; Hickman, J. J.; Boland, T. Inkjet printing of viable mammalian cells. *Biomaterials* **2005**, *26*, 93–99.
- Derby, B. Inkjet printing of functional and structural materials: fluid property requirements, feature stability, and resolution. *Annu. Rev. Mater. Res.* **2010**, *40*, 395–414.
- Boley, J. W.; White, E. L.; Chiu, G. T.-C.; Kramer, R. K. Direct writing of gallium-indium alloy for stretchable electronics. *Adv. Funct. Mater.* **2014**, *24*, 3501–3507.
- Yang, X.; Chhasatia, V. H.; Shah, J.; Sun, Y. Coalescence, evaporation and particle deposition of consecutively printed colloidal droplets. *Soft Matter* **2012**, *8*, 9205–9213.
- He, M.; Zhang, Q.; Zeng, X.; Cui, D.; Chen, J.; Li, H.; Wang, J.; Song, Y. Hierarchical porous surface for efficiently controlling microdroplets' self-removal. *Adv. Mater.* **2013**, *25*, 2291–2295.
- Kuang, M.; Wang, L.; Song, Y. Controllable printing droplets for high-resolution patterns. *Adv. Mater.* **2014**, *26*, 6950–6958.
- Piqué, A.; Chrisey, D. B. *Direct-Write Technologies for Rapid Prototyping Applications: Sensors, Electronics, and Integrated Power Sources*; Academic Press, 2001.
- Singh, M.; Haverinen, H. M.; Dhagat, P.; Jabbour, G. E. Inkjet printing process and its applications. *Adv. Mater.* **2010**, *22*, 673–685.
- Jiang, Y.; Hu, S.; Pan, Y. A Normalized Trace Geometry Modeling Method with Bulge-free Analysis for Direct Ink Writing Process Planning. *3D Printing and Additive Manufacturing*; Mary Ann Liebert, 2018.
- Son, Y.; Kim, C. Spreading of inkjet droplet of non-Newtonian fluid on solid surface with controlled contact angle at low Weber and Reynolds numbers. *J. Non-Newtonian Fluid Mech.* **2009**, *162*, 78–87.
- Wang, J. Z.; Zheng, Z. H.; Li, H. W.; Huck, W. T. S.; Sirringhaus, H. Dewetting of conducting polymer inkjet droplets on patterned surfaces. *Nat. Mater.* **2004**, *3*, 171–176.
- Vunnam, S.; Ankireddy, K.; Kellar, J.; Cross, W. Surface modification of indium tin oxide for direct writing of silver nanoparticulate ink micropatterns. *Thin Solid Films* **2013**, *531*, 294–301.
- Zheng, Y.; Zhang, Q.; Liu, J. Pervasive liquid metal based direct writing electronics with roller-ball pen. *APL Adv.* **2013**, *3*, 112117.
- Pascall, A. J.; Qian, F.; Wang, G.; Worsley, M. A.; Li, Y.; Kuntz, J. D. Light-directed electrophoretic deposition: A new additive manufacturing technique for arbitrarily patterned 3D composites. *Adv. Mater.* **2014**, *26*, 2252–2256.
- Liu, B.; Aydil, E. S. Growth of oriented single-crystalline rutile TiO<sub>2</sub> nanorods on transparent conducting substrates for dye-sensitized solar cells. *J. Am. Chem. Soc.* **2009**, *131*, 3985–3990.
- Gao, Y.; Li, H.; Liu, J. Direct writing of flexible electronics through room temperature liquid metal ink. *PLoS One* **2012**, *7*, No. e45485.
- Skylar-Scott, M. A.; Gunasekaran, S.; Lewis, J. A. Laser-assisted direct ink writing of planar and 3D metal architectures. *Proc. Natl. Acad. Sci. U.S.A.* **2016**, *113*, 6137–6142.
- Zhang, Q.; Zheng, Y.; Liu, J. Direct writing of electronics based on alloy and metal (DREAM) ink: A newly emerging area and its impact on energy, environment and health sciences. *Front. Energy* **2012**, *6*, 311–340.

- (37) Hu, J.; Yu, M.-F. Meniscus-confined three-dimensional electrodeposition for direct writing of wire bonds. *Science* **2010**, *329*, 313–316.
- (38) Derby, B. Inkjet printing ceramics: From drops to solid. *J. Eur. Ceram. Soc.* **2011**, *31*, 2543–2550.
- (39) Lewis, J. A. Direct-write assembly of ceramics from colloidal inks. *Curr. Opin. Solid State Mater. Sci.* **2002**, *6*, 245–250.
- (40) Smay, J. E.; Nadkarni, S. S.; Xu, J. Direct writing of dielectric ceramics and base metal electrodes. *Int. J. Appl. Ceram. Technol.* **2007**, *4*, 47–52.
- (41) Pierin, G.; Grotta, C.; Colombo, P.; Mattevi, C. Direct Ink Writing of micrometric SiOC ceramic structures using a preceramic polymer. *J. Eur. Ceram. Soc.* **2016**, *36*, 1589–1594.
- (42) Xu, M.; Gratson, G. M.; Duoss, E. B.; Shepherd, R. F.; Lewis, J. A. Biomimetic silicification of 3D polyamine-rich scaffolds assembled by direct ink writing. *Soft Matter* **2006**, *2*, 205–209.
- (43) Chen, B.; Jiang, Y.; Tang, X.; Pan, Y.; Hu, S. Fully packaged carbon nanotube supercapacitors by direct ink writing on flexible substrates. *ACS Appl. Mater. Interfaces* **2017**, *9*, 28433–28440.
- (44) Cheng, M.; Jiang, Y.; Yao, W.; Yuan, Y.; Deivanayagam, R.; Foroosan, T.; Huang, T.; Song, B.; Rojaee, R.; Shokuhfar, T.; Pan, Y.; Lu, J.; Shahbazian-Yassar, R. Elevated-temperature 3D Printing of hybrid solid-state electrolyte for Li-ion batteries. *Adv. Mater.* **2018**, *30*, 1800615.
- (45) Fonseca, C. P.; Cavalcante, F., Jr.; Amaral, F.; Souza, C. Z.; Neves, S. Thermal and conduction properties of a PCL-biodegradable gel polymer electrolyte with LiClO<sub>4</sub>, LiF<sub>3</sub>CSO<sub>3</sub>, and LiBF<sub>4</sub> salts. *Int. J. Electrochem. Sci.* **2007**, *2*, 52–63.
- (46) Jeong, S. S.; Lim, Y. T.; Choi, Y. J.; Cho, G. B.; Kim, K. W.; Ahn, H. J.; Cho, K. K. Electrochemical properties of lithium sulfur gels using PEO polymer electrolytes prepared under three different mixing conditions. *J. Power Sources* **2007**, *174*, 745–750.
- (47) Lu, L.; Zhang, Z.; Xu, J.; Pan, Y. 3D-printed polymer composites with acoustically assembled multidimensional filler networks for accelerated heat dissipation. *Composites, Part B* **2019**, *174*, 106991.
- (48) Joyee, E. B.; Lu, L.; Pan, Y. Analysis of mechanical behavior of 3D printed heterogeneous particle-polymer composites. *Composites, Part B* **2019**, *173*, 106840.
- (49) Peele, B. N.; Wallin, T. J.; Zhao, H.; Shepherd, R. F. 3D Printing antagonistic systems of artificial muscle using projection stereolithography. *Bioinspiration Biomimetics* **2015**, *10*, 055003.
- (50) Joyee, E. B.; Pan, Y. A Fully Three-dimensional printed inchworm-inspired soft robot with magnetic actuation. *Soft Robotics* **2019**, *6*, 333.
- (51) Shaffer, S.; Yang, K.; Vargas, J.; Di Prima, M. A.; Voit, W. On reducing anisotropy in 3D printed polymers via ionizing radiation. *Polymer* **2014**, *55*, 5969–5979.
- (52) Guo, Y.; Ji, Z.; Zhang, Y.; Wang, X.; Zhou, F. Solvent-free and photocurable polyimide inks for 3D printing. *J. Mater. Chem. A* **2017**, *5*, 16307–16314.
- (53) Zhang, J.; Xiao, P. 3D Printing of photopolymers. *Polym. Chem.* **2018**, *9*, 1530–1540.
- (54) He, Y.; Liu, Y.; Dyer, B. A.; Boone, J. M.; Liu, S.; Chen, T.; Zheng, F.; Zhu, Y.; Sun, Y.; Rong, Y.; Qiu, J. 3D-printed breast phantom for multi-purpose and multi-modality imaging. *Quant. Imaging Med. Surg.* **2019**, *9*, 63.
- (55) Liao, Y. L.; Chen, H. B.; Zhou, L. H.; Zhen, X. Construction of an anthropopathic abdominal phantom for accuracy validation of deformable image registration. *Technol. Health Care* **2016**, *24*, S717–S723.
- (56) Duan, B.; Hockaday, L. A.; Kang, K. H.; Butcher, J. T. 3D Bioprinting of heterogeneous aortic valve conduits with alginate/gelatin hydrogels. *J. Biomed. Mater. Res., Part A* **2013**, *101A*, 1255–1264.
- (57) Ng, W. L.; Yeong, W. Y.; Naing, M. W. Polyelectrolyte gelatin-chitosan hydrogel optimized for 3D bioprinting in skin tissue engineering. *Int. J. Bioprint.* **2016**, *2*, 53–62.
- (58) Liu, Z.; Zhang, M.; Bhandari, B.; Yang, C. Impact of rheological properties of mashed potatoes on 3D printing. *J. Food Eng.* **2018**, *220*, 76–82.
- (59) Yang, F.; Zhang, M.; Bhandari, B. Recent development in 3D food printing. *Crit. Rev. Food Sci. Nutr.* **2017**, *57*, 3145–3153.
- (60) Mohammed, M. G.; Kramer, R. All-printed flexible and stretchable electronics. *Adv. Mater.* **2017**, *29*, 1604965.
- (61) Wehner, M.; Truby, R. L.; Fitzgerald, D. J.; Mosadegh, B.; Whitesides, G. M.; Lewis, J. A.; Wood, R. J. An integrated design and fabrication strategy for entirely soft, autonomous robots. *Nature* **2016**, *536*, 451–455.
- (62) Trdine, J.; Handy, S. *Applications of Ionic Liquids in Science and Technology*; Intec: Rijeka, Croatia, 2011.
- (63) Nulwala, H.; Mirjafari, A.; Zhou, X. Ionic liquids and poly(ionic liquids) for 3D printing – A focused mini review. *Eur. Polym. J.* **2018**, *108*, 390–398.
- (64) Lagerwall, J. P. F.; Scalia, G. A new era for liquid crystal research: Applications of liquid crystals in soft matter nano-, bio- and microtechnology. *Curr. Appl. Phys.* **2012**, *12*, 1387–1412.
- (65) Hayati, I.; Bailey, A. I.; Tadros, T. F. Mechanism of stable jet formation in electrohydrodynamic atomization. *Nature* **1986**, *319*, 41–43.
- (66) Stevenin, C.; Béreaux, Y.; Charmeau, J. Y.; Balcaen, J. Shaping air flow characteristics of a high-speed rotary-bell sprayer for automotive painting processes. *J. Fluids Eng.* **2015**, *137*, 111304.
- (67) Barringer, S. A.; Sumonsiri, N. Electrostatic coating technologies for food processing. *Annu. Rev. Food Sci. Technol.* **2015**, *6*, 157–169.
- (68) Reynders, J. P.; Jandrell, I. R.; Reynders, S. M. Review of aging and recovery of silicone rubber insulation for outdoor use. *IEEE Trans. Dielectr. Electr. Insul.* **1999**, *6*, 620–631.
- (69) Wong, T.-S.; Kang, S. H.; Tang, S. K. Y.; Smythe, E. J.; Hatton, B. D.; Grinthal, A.; Aizenberg, J. Bioinspired self-repairing slippery surfaces with pressure-stable omniphobicity. *Nature* **2011**, *477*, 443–447.
- (70) Karniadakis, G.; Beskok, A.; Aluru, N. *Microflows and Nanoflows. Fundamentals and Simulation*; Springer: Berlin, 2005.
- (71) Lee, M. W.; Lathe, S. S.; Yarin, A. L.; Yoon, S. S. Dynamic electrowetting-on-dielectric (DEWOD) on unstretched and stretched Teflon. *Langmuir* **2013**, *29*, 7758–7767.
- (72) Yarin, A. L.; Roisman, I. V.; Tropea, C. *Collision Phenomena in Liquids and Solids*; Cambridge University Press: Cambridge, 2017.
- (73) Mugele, F.; Baret, J.-C. Electrowetting: from basics to applications. *J. Phys.: Condens. Matter* **2005**, *17*, R705–R774.
- (74) Lin, S.-W.; Keizer, J.; Rock, P. A.; Stenschke, H. On the mechanism of oscillations in the “beating” mercury heart. *Proc. Natl. Acad. Sci. U.S.A.* **1974**, *71*, 4477–4481.
- (75) Kumar, P.; Verma, D. K.; Parmananda, P.; Boccaletti, S. Experimental evidence of explosive synchronization in mercury beating-heart oscillators. *Phys. Rev. E: Stat., Nonlinear, Soft Matter Phys.* **2015**, *91*, 062909.
- (76) Yu, Z.; Chen, Y.; Yun, F. F.; Cortie, D.; Jiang, L.; Wang, X. Discovery of a voltage-stimulated heartbeat effect in droplets of liquid gallium. *Phys. Rev. Lett.* **2018**, *121*, 024302.
- (77) Beni, G.; Hackwood, S.; Jackel, J. L. Continuous electrowetting effect. *Appl. Phys. Lett.* **1982**, *40*, 912–914.
- (78) Verplanck, N.; Coffinier, Y.; Thomy, V.; Boukherroub, R. Wettability switching techniques on superhydrophobic surfaces. *Nanoscale Res. Lett.* **2007**, *2*, 577–596.
- (79) Zhao, Y.; Cho, S. K. Micro air bubble manipulation by electrowetting on dielectric (EWOD): transporting, splitting, merging and eliminating of bubbles. *Lab Chip* **2007**, *7*, 273–280.
- (80) Hayes, R. A.; Feenstra, B. J. Video-speed electronic paper based on electrowetting. *Nature* **2003**, *425*, 383–385.
- (81) Welters, W. J. J.; Fokkink, L. G. J. Fast electrically switchable capillary effects. *Langmuir* **1998**, *14*, 1535–1538.
- (82) Garrod, R. P.; Harris, L. G.; Schofield, W. C. E.; McGettrick, J.; Ward, L. J.; Teare, D. O. H.; Badyal, J. P. S. Mimicking a Stenocara beetle's back for microcondensation using plasmachemical patterned

superhydrophobic–superhydrophilic surfaces. *Langmuir* **2007**, *23*, 689–693.

(83) Kuiper, S.; Hendriks, B. H. W. Variable-focus liquid lens for miniature cameras. *Appl. Phys. Lett.* **2004**, *85*, 1128–1130.

(84) Yang, S.; Krupenkin, T. N.; Mach, P.; Chandross, E. A. Tunable and latchable liquid microlens with photopolymerizable components. *Adv. Mater.* **2003**, *15*, 940–943.

(85) Dubois, P.; Marchand, G.; Fouillet, Y.; Berthier, J.; Douki, T.; Hassine, F.; Gmouh, S.; Vaultier, M. Ionic liquid drop as e-microreactor. *Anal. Chem.* **2006**, *78*, 4909–4917.

(86) Rioboo, R.; Tropea, C.; Marengo, M. Outcomes from a drop impact on solid surfaces. *Atomization Sprays* **2001**, *11*, 155–166.

(87) Schiaffino, S.; Sonin, A. A. Molten droplet deposition and solidification at low Weber numbers. *Phys. Fluids A* **1997**, *9*, 3172–3187.

(88) Rioboo, R.; Marengo, M.; Tropea, C. Time evolution of liquid drop impact onto solid, dry surfaces. *Exp. Fluids* **2002**, *33*, 112–124.

(89) Theron, S. A.; Zussman, E. Electric and magnetic parameters of liquids and gases. In *Springer Handbook of Experimental Fluid Mechanics*; Springer: Berlin, 2007; Chapter 3.7.

(90) Yarin, A. L.; Lee, M. W.; An, S.; Yoon, S. S. *Self-Healing Nanotextured Vascular Engineering Materials*; Springer Nature: Switzerland AG, 2019.

(91) Reznik, S. N.; Yarin, A. L.; Zussman, E.; Bercovici, L. Evolution of a compound droplet attached to a core-shell nozzle under the action of a strong electric field. *Phys. Fluids* **2006**, *18*, 062101.

(92) Kistler, S. F. Hydrodynamics of wetting. In *Wettability*; Berg, J. C., Ed.; Marcel Dekker: New York, 1993; pp 311–429.

(93) Yurkiv, V.; Yarin, A. L.; Mashayek, F. Modeling of droplet impact onto polarized and non-polarized dielectric surfaces. *Langmuir* **2018**, *34*, 10169–10180.

(94) Hinton, T. J.; Hudson, A.; Pusch, K.; Lee, A.; Feinberg, A. W. 3D Printing PDMS elastomer in a hydrophilic support bath via freeform reversible embedding. *ACS Biomater. Sci. Eng.* **2016**, *2*, 1781–1786.

(95) Roh, S.; Parekh, D. P.; Bharti, B.; Stoyanov, S. D.; Velez, O. D. 3D printing by multiphase silicone/water capillary inks. *Adv. Mater.* **2017**, *29*, 1701554.

(96) Ozbolat, V.; Dey, M.; Ayan, B.; Povilianskas, A.; Demirel, M. C.; Ozbolat, I. T. 3D Printing of PDMS improves its mechanical and cell adhesion properties. *ACS Biomater. Sci. Eng.* **2018**, *4*, 682–693.

(97) Zhou, L.-y.; Gao, Q.; Fu, J.-z.; Chen, Q.-y.; Zhu, J.-p.; Sun, Y.; He, Y. Multi-material 3D printing of highly stretchable silicone elastomer. *ACS Appl. Mater. Interfaces* **2019**, *11*, 23573–23583.

(98) Zussman, E.; Yarin, A. L.; Nagler, R. M. Age- and flow-dependency of salivary viscoelasticity. *J. Dent. Res.* **2007**, *86*, 281–285.

(99) Reneker, D. H.; Yarin, A. L.; Zussman, E.; Xu, H. Electrospinning of nanofibers from polymer solutions and melts. *Advances in Applied Mechanics*; Elsevier, 2007; Vol. 41, pp 43–195.

(100) Yarin, A. L.; Pourdeyhimi, B.; Ramakrishna, S. *Fundamentals and Applications of Micro- and Nanofibers*; Cambridge University Press: Cambridge, 2014.

(101) Yarin, A. L.; Zussman, E.; Theron, A.; Rahimi, S.; Sobe, Z.; Hasan, D. Elongational behavior of gelled propellant simulants. *J. Rheol.* **2004**, *48*, 101–116.

(102) Löwe, J. M.; Secklehner, M.; Hinrichsen, V. Investigation of surface charges on polymeric insulators and the influence of sessile water droplets. *Electrical Insulation Conference (INSUCON). 2017, INSUCON-13th International*; IEEE, pp 1–7.

(103) Choi, D.; Lee, H.; Kang, I. S.; Lim, G.; Kim, D. S.; Kang, K. H. Spontaneous electrical charging of drops by conventional pipetting. *Sci. Rep.* **2013**, *3*, 2037.

(104) Liu, Y. J.; Liao, T. Y.; Joseph, D. D. A two-dimensional cusp at the trailing edge of an air bubble rising in a viscoelastic liquid. *J. Fluid Mech.* **1995**, *304*, 321–342.